FREQUENCY RESPONSE OF THIN TOROIDAL INDUCTORS: A HYBRID APPROACH COMBINING THEORY, SIMULATION AND MEASUREMENT

Manuscript Info

Manuscript History

Key words: -

Thin toroidal inductor, frequency response, hybrid modeling, experimental characterization, Highfrequency optimisation.

Abstract

This paperinvestigates the frequency response of a thintoroidalinductor (200 $\,\mu m)$ made of 4C65 ferrite and wound with 18 turns. A hybridmethodology combininganalytical modeling, numerical simulation using HFSS, and experimental characterization with a 6500B impedance analyzer. The analysis focuses on two key parameters: the self-inductance (L) and the series resistance (R) as functions of frequency.

The comparative studybetweentheoretical, simulated, and measuredresults demonstrates that the inductance remains close to 1 μH over the 1 MHz–10 MHz range. The DC resistance (R_{DC}) is approximately 12 m Ω , while the simulated and measured AC resistances (R_{AC}) exhibit good agreement. However, analytical models show noticeabled eviations beyond approximately 1 MHz, revealing their limitations in predicting high-frequency behavior.

Copy Right, IJAR, 2019,. All rights reserved.

Introduction: -

- 2 Modern power electronicsisincreasinglyshiftingtoward compact, high-performance components designed for high-
- 3 frequencyoperation. In this context, toroidal magnetic-core inductors, particularly those with reduced thickness,
- 4 offerstrongpotential for integration. However, theirelectromagnetic behavior becomes complex to model,
- 5 especiallywhen high-frequencyeffectssuch as skin effect, proximityeffect, and parasitic capacitances come intoplay.
- 6 This work proposes a systematic approach for analyzing the magnetic component, combining theoretical modeling,
- 7 numerical simulation, and experimental characterization. Through the study of a toroidal component made of NiZn
- 8 ferrite (4C65 material), the objective is to betterpredictitsfrequencybehavior and derive relevant models for future
- 9 optimized inductor designs.

10

11 12

13

14 15

16

1

I. METHODOLOGY AND MATERIALS

The methodology proposed in this study consists of characterizing a toroidal inductor with a magnetic core by measuring its inductance and series resistance using a 6500B impedance analyzer. A hybrid approach combining analytical calculations, numerical simulations, and experimental measurements is implemented to provide a comprehensive understanding of the component's frequency-dependent behavior.

A. Target Structure and Component Parameters

- 17 The target structure (Figure 1) is a toroidal inductor (NiZn ferrite, 4C65) with a closed rectangular-shaped cross-
- section and a reduced thickness of approximately 200 µm. The conductor used is an enameled copper wire with a
- 19 circular cross-section.

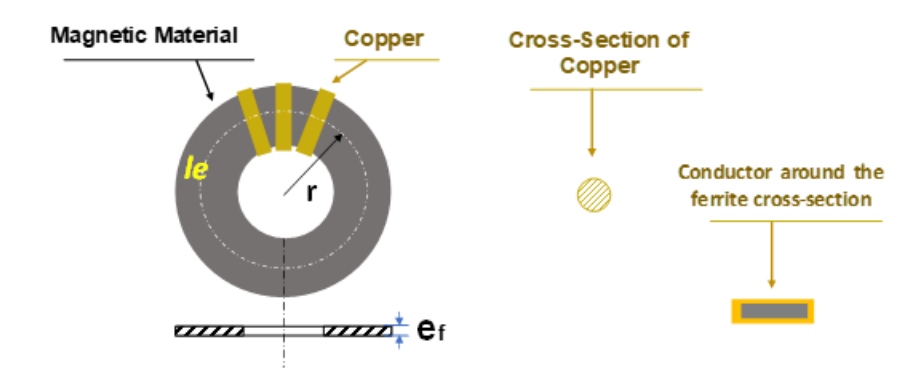


Figure 1: Target Structure and Parameters.

The component's characteristics are summarized in the following table:

Table 1: Component Characteristics

Symbol	Value	Unit
d_o/d_i	36.25/22.75	mm
A	6.75 x 0.20	mm²
-1 _e	89.7	mm
μ_{i}	125	-
S_{Cu}	0.44	mm²
N	18	
1	311	mm
	$\begin{matrix} d_{o}/d_{i} \\ A \\ l_{e} \\ \mu_{i} \\ S_{Cu} \end{matrix}$	$\begin{array}{c ccccccccccccccccccccccccccccccccccc$

B. Analytical Models

1) Self-Inductance Coefficient L

For a toroidal structure with a closed magnetic circuit, the analytical model of the inductance L depends on the relative permeability μ r of the magnetic material, the number of turns N, and the geometric parameters of the magnetic core.

30 Conventionally, this value is calculated using the following formula:

$$L = \mu_r \mu_0 N^2 \frac{A_e}{l_e} = \mu_r \mu_0 N^2 \frac{A_e}{\pi (r_i + r_0)}$$
 [H] (1)

where μ_r and μ_0 are the relative permeability of the material and of vacuum, respectively ($\mu_0 = 4\pi \times 10^{-7} \, \text{H/m}$).

For thin components such as integrated inductors, the magnetic circuit has a square cross-section, as in our case, with relatively small thicknesses (ranging from a few tens to several hundred micrometers). To predict the inductance of such components, some authors [1] use the following logarithmic formula:

$$L_{core} = \mu_r \mu_0 N^2 \frac{t_{core}}{2\pi} ln \left(\frac{d_o}{d_i}\right)$$
 [H] (2)

37 Where t_{core} represents the thickness of the magnetic circuit.

The adaptation of these two models to our component, considering a frequency-dependent permeability, yields the following results:

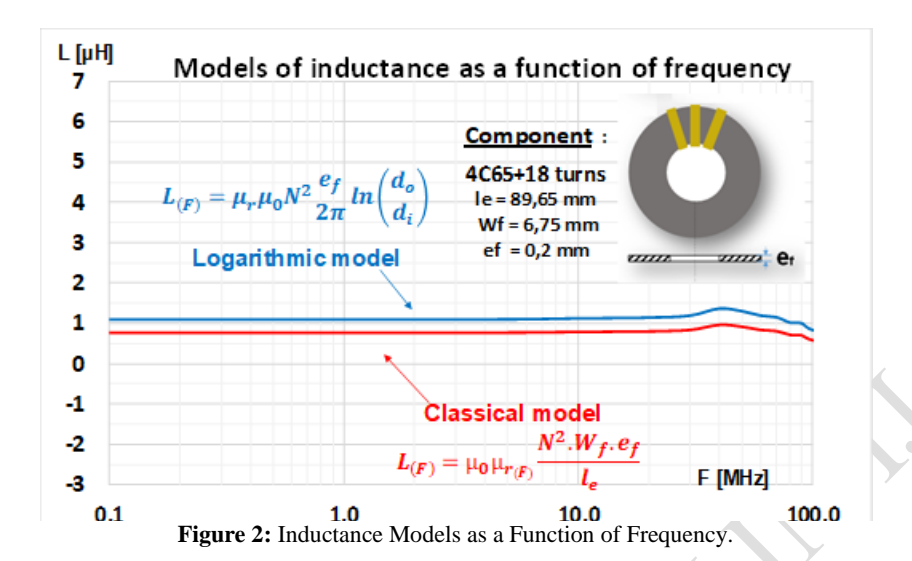


Figure 2 shows that the inductance remains nearly constant from 100 kHz up to several tens of MHz, corresponding to the linear operating region of the magnetic circuit. It should be noted that the logarithmic model predicts inductance values approximately $0.3 \, \mu\text{H}$ higher than those obtained with the classical model.

2) Series Resistance R

The series resistance accounts for the DC resistance (RDC) of the conductor, the influence of the magnetic material's resistivity, and the skin and proximity effects, which become significant at high frequencies.

The DC resistance, or low-frequency resistance, is the main source of copper losses, as it dissipates energy in the form of heat. It can be calculated from the resistivity ρ of the conductor, its cross-sectional area S_{Cu} , and its total length l, as follows:

$$R_{DC} = \rho_{Cu} \frac{l}{S_{Cu}} \quad [\Omega]$$
 (3)

With the resistivity of copper being $\rho \approx 1.68 \times 10^{-8} \,\Omega$ ·m, applying this formula yields $R_{DC} \approx 12 \,\mathrm{m}\Omega$.

a) Skin Effect

When the conductor carries a time-varying current (Figure 3), it generates a varying magnetic field around it. Variations in this field induce eddy currents toward the periphery of the conductor. Part of this current flows preferentially (in the same direction as the main current) within a depth δ , known as the skin depth. As a result, the effective cross-section of the conductor decreases, increasing its resistance.

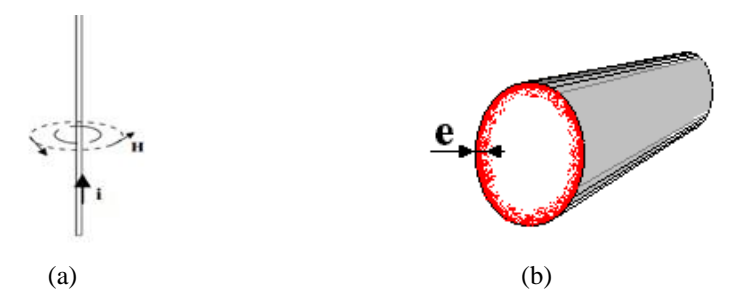


Figure 3: Skin Effect: (a) Effect of the current i(t) in a conductor; (b) Skin depth (δ) [2].

The skin depth is calculated as follows:

$$\delta = \sqrt{\frac{\rho}{\mu_0 \mu_r \pi f}} \simeq \frac{66}{\sqrt{f}} [\mu m] \quad (4)$$

63 where μ_r is the relative permeability of copper (μ_r = 1) and f is expressed in MHz.

- $\delta \simeq 29 \,\mu\text{m}@5 \,\text{MHz}$, a value more than 12 times smaller than the diameter of the copper used for the fabrication of our component. The effective cross-section of the copper is thus reduced from 0.44 mm² to 0.07 mm² (i.e., S_{Cv}/6), a reduction that increases the resistance at 5 MHz by a factor of approximately 6.
- 67 Two models in the literature [3], [4] that incorporate the skin effect are particularly noteworthy:
- $R_{(f)} = R_{DC} \left[1 + \frac{d}{s} \right]$ 68 Snelling Model:

64

65

66

70

71

73 74

75

76

77

78

79

80

81

82

83

84

- $R_{(f)} = R_{DC} \left[1 + \frac{(r_0/\delta)^4}{48 + 0.8(r_0/\delta)^4} \right]$ (6) 69 Hurley Model:
 - where d represents the diameter of the copper and r_0 represents the radius of the copper.
- Although slightly different, these formulas share the common feature of accounting for the skin depth. Their 72 implementation yields the following result:

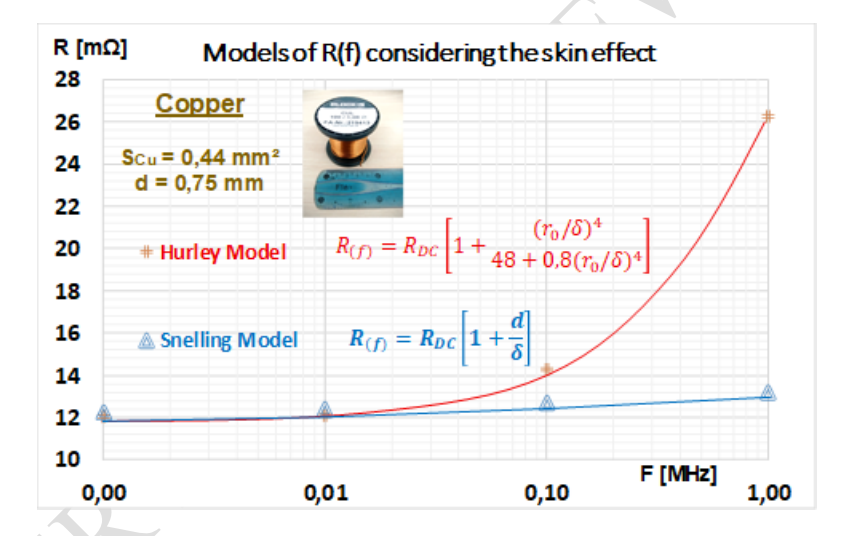


Figure 4: Models of R(f) Considering the Skin Effect.

This result shows that Hurley's model predicts a faster increase in resistance starting from 10 kHz, whereas Snelling's model keeps the resistance almost constant up to 1 MHz.

b) Consideration of the proximity effect and parasitic capacitances

The proximity effect (Figure 5a) occurs when neighboring conductors carry alternating currents. For instance, when two conductors are placed side by side and one carries an AC current, it generates a varying magnetic field that can induce a current in the second conductor, and vice versa. These induced currents circulate in both conductors, which may lead to additional copper losses.

Moreover, parasitic capacitances arise from capacitive coupling between adjacent turns and between the turns and the magnetic core. These effects become significant at high frequencies. Charles R. Sullivan et al. [5] illustrated these parasitic capacitances as shown in Figure 5b.

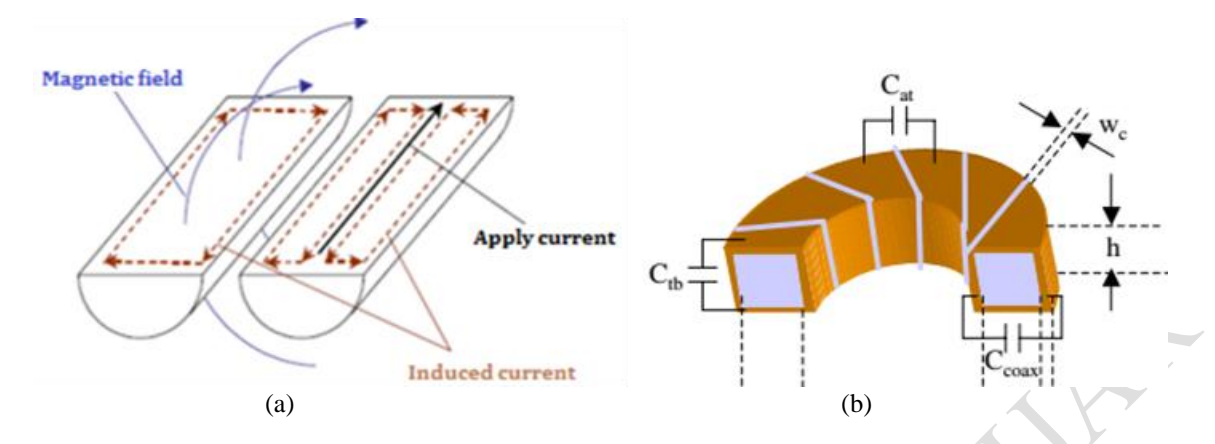


Figure 5: (a) Principle of the Proximity Effect [6]; (b) Parasitic capacitances in toroidal inductors [5].

In the literature, the model by Kuhn et al. [7] is explicit in this regard, incorporating the spacing s between turns, the conductor thickness e, and the conductor width w to empirically account for these parameters, as follows:

$$R_{(f)} = R_{DC} \left[1 + 0.1 \left(\frac{2\pi f}{\omega_{crit}} \right)^2 \right] = R_{DC} \left[1 + 0.1 \left(\frac{2\pi f}{\frac{3.1(w + S) \rho_{Cu}}{\mu_{0} w^2} \cdot \frac{e^2}{e}} \right)^2 \right]$$
(7)

91 For a conductor with a circular cross-section, the equivalent thickness w is expressed as:

$$92 w = (d\sqrt{\pi})/2 (8)$$

Recently, Zhao et al. [8] proposed a more advanced formulation for inductors with m layers of conductors wound on top of each other around a toroidal magnetic core. For a winding layer of N turns with diameter d around a ferrite core of inner radius r, subjected to a magnetic excitation H produced by a current I, the formulation can be summarized as:

97
$$\frac{R_{AC(f)}}{R_{DC}} = \frac{\gamma}{2} \left[\varphi_{1(\gamma)} + \left(\frac{4\pi rH}{NI} \right)^2 \varphi_{2(\gamma)} \right] - \frac{\xi}{\sqrt{2}} \left[\left(\frac{2\sqrt{\pi}Hd}{I} \right)^2 \psi_{3(\xi)} \right]$$
(9)

98 The first term of Equation (9) is derived from the modified Dowell method as follows:

$$\varphi_{1(\gamma)} = \frac{\sinh(\gamma) + \sin(\gamma)}{\cosh(\gamma) - \cos(\gamma)} \tag{10}$$

100
$$\varphi_{2(\gamma)} = \frac{\sinh(\gamma) - \sin(\gamma)}{\cosh(\gamma) + \cos(\gamma)}$$
 (11)

The second term of the equation corresponds to the modified Ferreira model:

$$\xi = \frac{d\sqrt{2\pi f \,\mu_0 \sigma}}{2} \tag{12}$$

103
$$\psi_{3(\xi)} = \frac{ber_1(bei_2 + ber_2) + bei_1(bei_2 - ber_2)}{bei_1^2 + ber_1^2}$$
 (13)

104 It should be noted that:

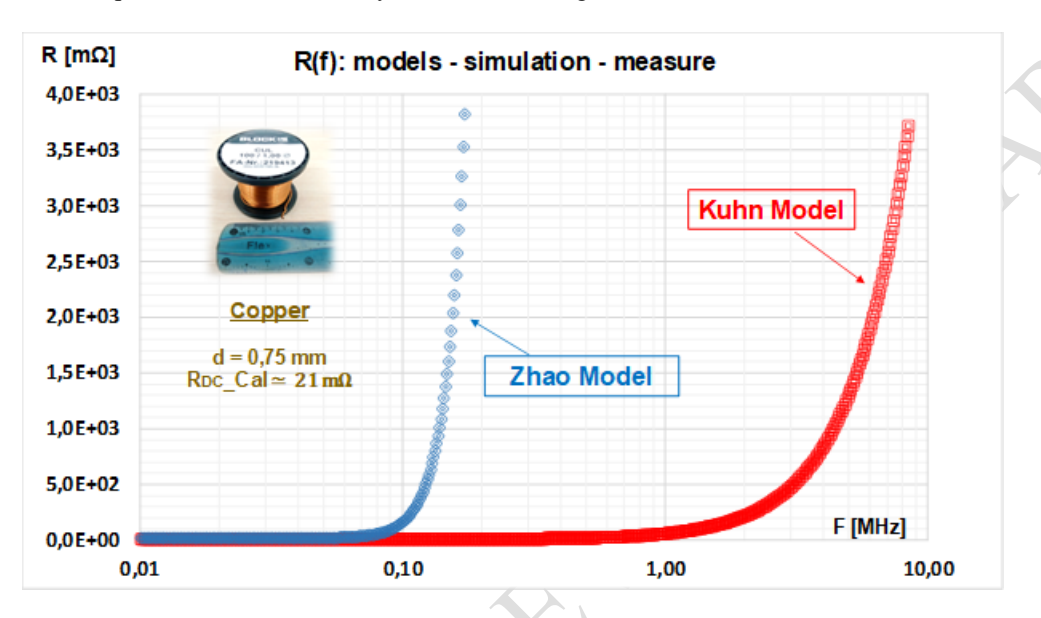
$$ber_{v} = ber_{v}(\xi) \tag{14}$$

 $bei_v = bei_v(\xi) \tag{15}$

ber_v and bei_v are, respectively, the Kelvin functions of order v.

For implementation purposes, the Kelvin functions can be approximated using a Taylor series expansion.

The application of Equations (7), (8), and (9) yields the following results:



110111

112

113

114

115116

117

118

119

120

109

Figure 6: Comparison of Analytical Models of R(f).

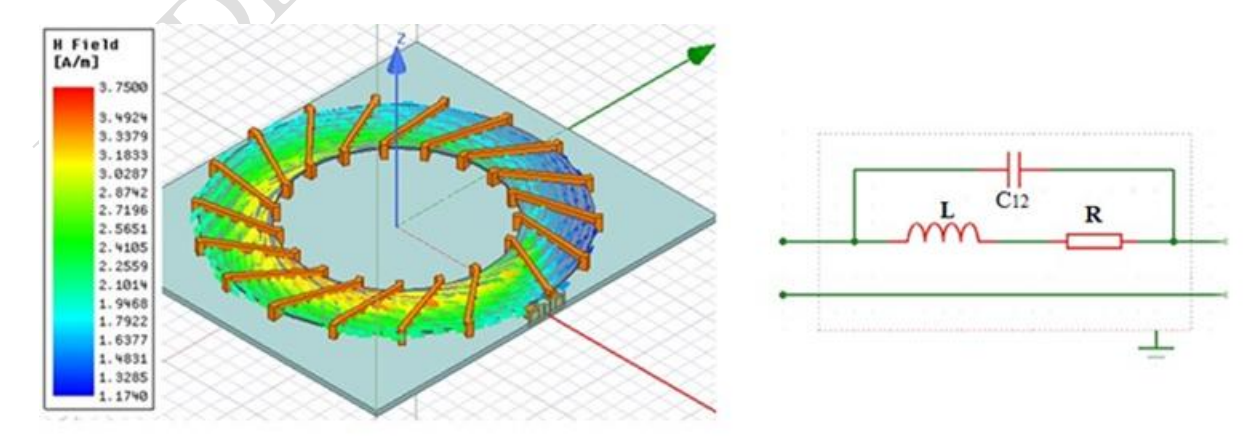
These models account for the influence of frequency on the component's series resistance. However, Zhao's model rises faster than Kuhn's model. Consequently, experimental validation is required to fully confirm their accuracy.

C. Simulation

The component was simulated using HFSS (High-Frequency Structure Simulator), a 3D electromagnetic software from Ansys, designed for high-frequency field analysis. It relies on the Finite Element Method (FEM) to solve Maxwell's equations in complex geometries.

1) Simulated Component and Extraction Model

A 3D model of the component was created in HFSS, as shown in Figure 7. The figure illustrates the simulated component, the associated magnetic field distribution, and its behavior under low-amplitude excitation.



122 (a)

123 Figure 7: (a) Simulated Component; (b) Extraction Model.

The simulations were performed in the frequency domain, with extraction of the R and L parameters according to the RLC model shown in Figure 7b. For the determination of the model parameters, the admittance parameters Yij are used. Let:

$$R = \frac{-Re(\underline{y}_{12})}{\left[Re(\underline{y}_{12})\right]^2 + \left[Im(\underline{y}_{12} + C_{12}\omega)\right]^2}$$
(16)

128
$$L = \frac{lm(\underline{y}_{12}) + C_{12}\omega}{\omega \left[Re(\underline{y}_{12})\right]^2 + \left[lm(\underline{y}_{12} + C_{12}\omega)\right]^2}$$
(17)

129 With
$$C_{12} = \frac{1}{(2f_0\pi)^2 L_0}$$
 (18)

130 The inductance L₀ is extracted in the low-frequency domain, where the component behaves mainly as an inductor.

The resonance frequency fo is determined from the frequency analysis of the imaginary part of the admittance Y12. It

132 corresponds to the frequency at which $Im(Y_{12}) = 0$.

2) Simulation Parameters

131

133

134

135

136

137138

139 140

141

142

143144

The key parameters summarized in the following table are used for the simulation:

Table 2: Simulation Parameters

Catégory	Parameter Name	Value	Description
Setup	Number of Passes	99	Maximum number of meshrefinement passes
	ΔS	5e-5	Convergence criterion for S-parameters
Sweep	Frequency	20 Hz-300 MHz	Simulation frequency range
	Number of Points	1000	Samples per frequencysweep

D. Materials and experimental setup

1) Test Component

The tested component (Figure 8(g)) consists of a NiZn ferrite toroid (4C65) wound with an enameled copper wire with a 0.75 mm diameter. The toroid is first manually ground to reduce its thickness from 15 mm to approximately 1 mm, then bonded to a glass substrate (60 mm \times 45 mm) using Canada balsam under gentle heating. After 24 hours of drying, an automatic grinding process further reduces the ferrite thickness to about 200 μ m. The sample is then heated to 120 °C to detach the ferrite. Due to its fragility, a protective PLA casing (Figure 8(f)) is 3D-printed to improve mechanical stability during handling.

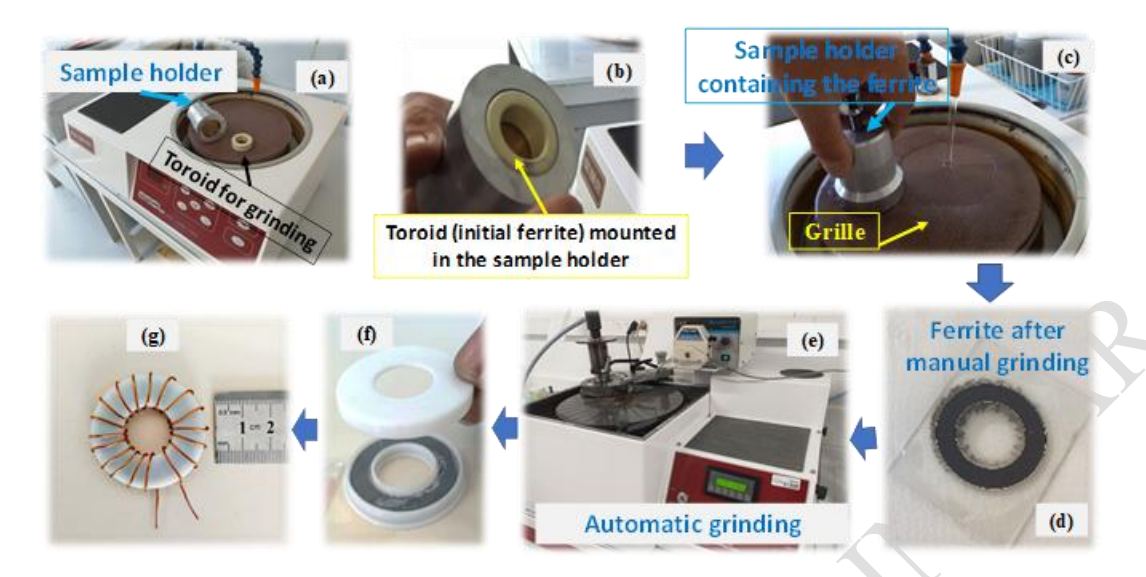


Figure 8: Fabrication of the test component: (a) manual grinder; (b) initial toroid in the sample holder; (c) manual grinding; (d) toroid prepared for automatic grinding; (e) automatic grinder; (f) toroid in 3D-printed casing; (g) test component (4C65 + 18 turns).

1) Measurement Setup

The experimental setup (Figure 9) uses a 6500B impedance analyzer connected to the test component through a model 1011 test fixture. This instrument allows measurements over a 20 Hz – 120 MHz frequency range. Calibration is essential for ensuring accuracy, and the available calibration modes enable appropriate determination of the electrical parameters (L and R). A computer is employed for data acquisition, processing, and comparison between analytical and simulated results.

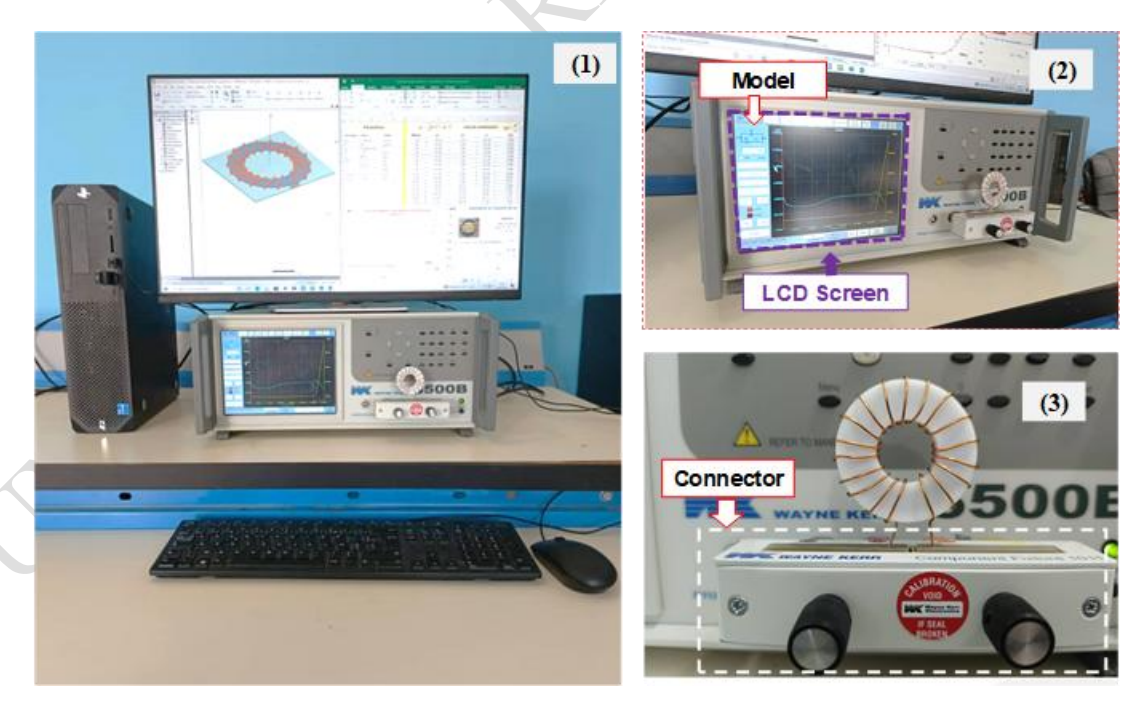


Figure 9: (1) Measurement setup: (2) impedance analyzer (6500B), (3) device under test (DUT).

II. RESULTS AND ANALYSIS

A. Inductance L(f)

The obtained curves (Figure 10) are consistent in the frequency range between 100 kHz and 10 MHz. The analytical, simulated, and measured results exhibit satisfactory agreement within this frequency band.

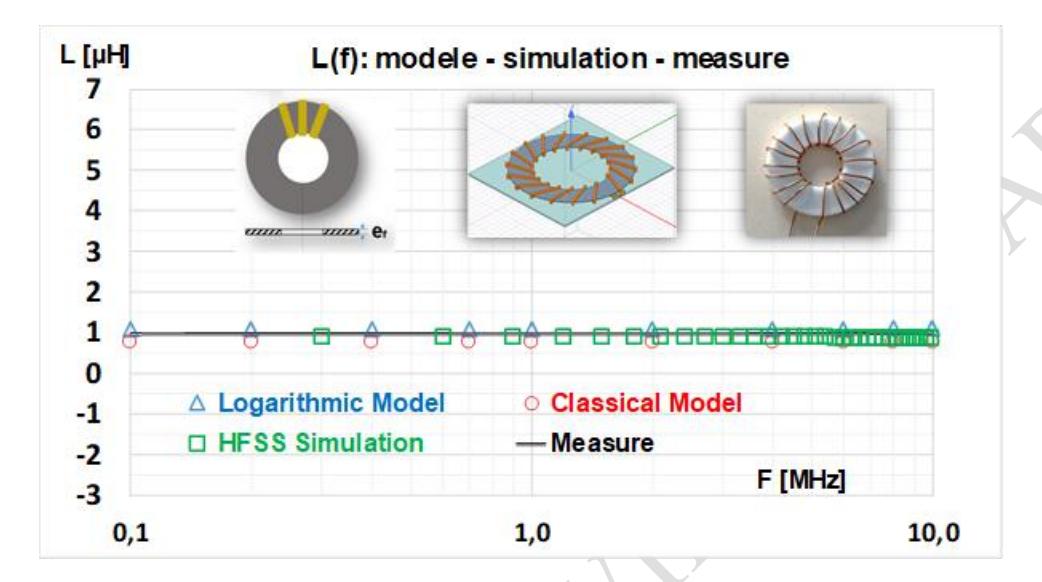


Figure 10: Comparison of inductance results as a function of frequency.

The measurements indicate that, over this frequency range, the inductance value is approximately the average of the two models.

B. Series Resistance R(f)

The measured and simulated results of the component's series resistance as a function of frequency, compared with analytical models, are shown in Figure 11.

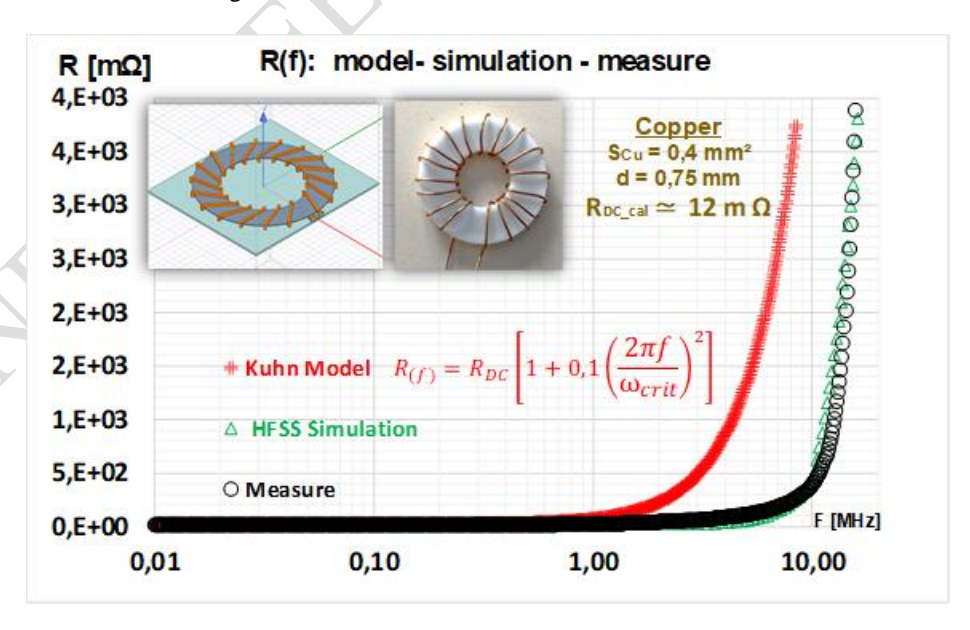


Figure 11: Comparison of series resistance results as a function of frequency.

- 170 The results indicate good agreement between measurements and simulations. However, Kuhn's analytical model
- fails to accurately predict the series resistance R(f), highlighting the inherent limitations of analytical approaches at
- high frequencies.
- 173 III. DISCUSSION
- 174 The obtained results confirm the complementarity of the approaches employed. Up to 10 MHz, the three methods
- 175 converge: the analytical model, HFSS simulation, and measurements all show consistent inductance values.
- However, beyond this threshold, the nonlinearity of the magnetic material, as well as capacitive effects, affect this
- 177 agreement. Regarding the series resistance, Kuhn's model incorporate the skin and proximity effects but do not
- match our measurements, except at low frequencies. The influence of skin depth, turn spacing, and parasitic
- capacitances is thus highlighted, emphasizing the importance of both optimizing the winding geometry and
- developing a more suitable R(f) model for high-frequency applications.
- 181 IV. CONCLUSION
- This work made possible the characterization of a thin toroidal inductor through a threefold approach: analytical,
- numerical, and experimental. The study showed a good agreement between the models and measurements for L(f)
- up to 10 MHz. In contrast, for R(f), only measurements or simulations allow accurate modeling, taking into account
- the inter-turn capacitance. These results provide concrete avenues for optimization, such as developing a simple and
- low-cost R(f) model.

187

- 188 V. REFERENCES
- 189 [1] X. Yu, J. Kim, F. Herrault, et M. G. Allen, « Silicon-embedded toroidal inductors with magnetic cores: Design
- methodology and experimental validation », in 2014 IEEE Applied Power Electronics Conference and Exposition APEC 2014, Fort Worth, TX, USA: IEEE, mars 2014, p. 763-767. doi:
- 192 10.1109/APEC.2014.6803394.
- 193 [2] D. D. Yaya, « Conception, réalisation et caractérisation d'inductances planaires à couches magnétiques ».
- 194 [3] W. G. Hurley et W. H. Wölfle, Transformers and inductors for power electronics: theory, design and
- 195 applications. John Wiley & Sons, 2013. Consulté le: 27 octobre 2025. [En ligne]. Disponible sur:
- 196 10.1002/9781118544648
- 197 [4] E. C. (Eric C. Snelling, *Soft ferrites: properties and applications*. Iliffe, 1969. Consulté le: 27 octobre 2025. [En
- ligne]. Disponible sur: https://cir.nii.ac.jp/crid/1971430859790257689
- 199 [5] C. R. Sullivan, W. Li, S. Prabhakaran, et S. Lu, « Design and Fabrication of Low-Loss Toroidal Air-Core
- 200 Inductors », in 2007 IEEE Power Electronics Specialists Conference, Orlando, FL, USA: IEEE, 2007, p.
- 201 1754-1759. doi: 10.1109/PESC.2007.4342265.
- 202 [6] A. A. Abderahim, « Etude des pertes dans les enroulements des composants passifs planaires ».
- 203 [7] W. B. Kuhn et N. M. Ibrahim, « Analysis of current crowding effects in multiturn spiral inductors », *IEEE Trans. Microw. Theory Tech.*, vol. 49, n° 1, p. 31-38, janv. 2001, doi: 10.1109/22.899959.
- 205 [8] Y. Zhao, Z. Ming, et B. Han, « Analytical modelling of high-frequency losses in toroidal inductors », *IET Power Electron.*, vol. 16, n° 9, p. 1538-1547, juill. 2023, doi: 10.1049/pel2.12493.